

Introspective Deep Metric Learning for Image Retrieval

Wenzhao Zheng* Chengkun Wang* Jie Zhou Jiwen Lu†

Beijing National Research Center for Information Science and Technology, China

Department of Automation, Tsinghua University, China

{zhengwz18, wck20}@mails.tsinghua.edu.cn; {jzhou, lujiwen}@tsinghua.edu.cn

Abstract

This paper proposes an introspective deep metric learning (IDML) framework for uncertainty-aware comparisons of images. Conventional deep metric learning methods produce confident semantic distances between images regardless of the uncertainty level. However, we argue that a good similarity model should consider the semantic discrepancies with caution to better deal with ambiguous images for more robust training. To achieve this, we propose to represent an image using not only a semantic embedding but also an accompanying uncertainty embedding, which describes the semantic characteristics and ambiguity of an image, respectively. We further propose an introspective similarity metric to make similarity judgments between images considering both their semantic differences and ambiguities. The proposed IDML framework improves the performance of deep metric learning through uncertainty modeling and attains state-of-the-art results on the widely used CUB-200-2011, Cars196, and Stanford Online Products datasets for image retrieval and clustering. We further provide an in-depth analysis of our framework to demonstrate the effectiveness and reliability of IDML. Code is available at: <https://github.com/wzzheng/IDML>.

1. Introduction

Learning an effective metric to measure the similarity between data is a long-standing problem in computer vision, which serves as a fundamental step in various downstream tasks, such as face recognition [12, 39, 60], image retrieval [1, 43, 76] and image classification [8, 41]. The objective of metric learning is to reduce the distances between positive pairs and enlarge the distances between negative pairs, which has recently powered the rapid developments for both supervised learning [57, 78] and unsupervised learning [4, 5, 11, 14].

*Equal contribution.

†Corresponding author.

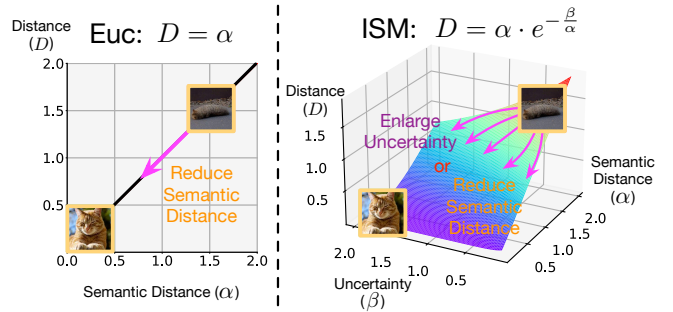


Figure 1. For a semantically ambiguous image, conventional DML explicitly reduces its distance with other intraclass images unaware of the uncertainty. Differently, the proposed introspective similarity metric provides an alternative way to enlarge the uncertainty level to allow confusion in the network.

Generally, deep metric learning (DML) employs deep neural networks [15, 42, 46] to map an image to a discriminative embedding space [70]. Most methods represent images using a deterministic embedding which only describes the characteristic features [39, 58]. Nevertheless, when asked to classify a certain image, humans are able to additionally provide the corresponding confidence as well as the semantic features of the image since an image might be ambiguous. Motivated by this, researchers have proposed a variety of probabilistic embedding methods using distributions to model images in the embedding space [7, 32, 44, 67]. They typically use KL-divergence [16] or Monte-Carlo-sampling-based [32] distances to measure the similarity between images. They regard the variance of the distributions as the uncertainty measure of images, yet they still provide a confident judgment of similarity regardless of the uncertainty. Specifically, though the variance affects the distribution discrepancy, a larger variance of an image does not necessarily blur its differences from other images. Given a highly ambiguous image (e.g., an extremely blurred image), we think it is more reasonable to weaken the semantic discrepancies and consider it similar to other images since it literally could be anything.

In this paper, we propose an introspective similarity metric to achieve this and further present an introspective deep

metric learning (IDML) framework for image retrieval. Different from existing methods, we represent an image using a semantic embedding to capture the semantic characteristics and further accompany it with an uncertainty embedding to model the uncertainty. An introspective similarity metric then takes as input both embeddings and outputs an uncertainty-aware similarity score, which softens the semantic discrepancies by the degree of uncertainty. Different from the conventional metric, the proposed introspective metric deems a pair of images similar if they are either semantically similar or ambiguous to judge, as illustrated in Figure 1. It provides more flexibility to the training process to avoid the harmful influence of inaccurately labeled data. To further demonstrate the advantage of the proposed metric for learning with uncertainties, we employ the widely used Mixup [6, 49, 69] technique to generate images with large uncertainties and further employ the IDML framework for learning. The overall framework of the proposed IDML can be trained efficiently in an end-to-end manner and generally applied to existing deep metric learning methods. We perform extensive experiments on the CUB-200-2011, Cars196, and Stanford Online Products datasets for image retrieval, which shows that our framework generally improves the performance of existing deep metric learning methods by a large margin and attains state-of-the-art results. We additionally provide an in-depth analysis of our framework including an ablation study of different components, effects of different augmentations, and qualitative analysis of the learned uncertainty.

2. Related Work

Deep Metric Learning: Deep metric learning aims to construct an effective embedding space to measure the similarity between images. The objective is to decrease intraclass distances and increase interclass distances. Most methods [2, 8, 9, 18, 22, 27, 43, 52–55, 62, 68, 73] employ a discriminative loss to learn the image embeddings. For example, the commonly used contrastive loss [18] pulls embeddings from the same class as close as possible while maintaining a fixed margin between embeddings from different classes. Wang *et al.* [55] further formulated three types of similarities between embeddings and proposed a multi-similarity loss to restrict them. The ProxyNCA loss [27] generates a proxy for each class and instead constrains the distances between embeddings and proxies.

In addition to the design of loss functions, various methods have explored effective sampling strategies for better training [10, 13, 39, 58, 65, 66, 69, 74]. For example, hard negative mining [13, 39, 65] selects challenging negative samples for more efficient learning of the metric. To further alleviate the lack of informative training samples, recent works [10, 75] proposed to generate synthetic samples for training. Also, a variety of data augmentation methods im-

prove the performance by mixing original images for better generalization [66, 69]. The aforementioned methods employ synthetic images for training, which can be semantically ambiguous. We design an introspective similarity metric to consider the uncertainty and further incorporate them to make similarity judgments.

Uncertainty Modeling: Uncertainty modeling is widely adopted in natural language processing to model the inherent hierarchies of words [29, 30, 50]. Vilnis *et al.* [50] proposed the Gaussian formation in word embedding and Nguyen *et al.* [30] presented a mixture model to learn multi-sense word embeddings. The computer vision field has also benefited from uncertainty modeling due to the natural uncertainty in images caused by various factors such as occlusion and blur [21, 40]. Various methods have attempted to model the uncertainty for better robustness and generalization in face recognition [3, 41], point cloud segmentation [67], and age estimation [25].

A prevailing method is to model each image as a statistical distribution and regard the variance as the uncertainty measure. For example, Oh *et al.* [32] employed Gaussian distributions to represent images and used Monte-Carlo sampling to sample several point embeddings from the distributions. They then imposed a soft contrastive loss on the sampled embeddings to optimize the metric. Similar strategy has also been used in pose estimation [44], cross-model retrieval [7] and unsupervised embedding learning [61]. However, they still make confident similarity judgments regardless of the uncertainty and a larger variance would not necessarily weaken the semantic discrepancies between samples. Differently, we propose an introspective metric to measure the similarity between images, which tends to omit the semantic differences between two images given a large uncertainty level. Also, our method bypasses the optimization of distributions to further increase the robustness.

3. Proposed Approach

3.1. Motivation of an Uncertainty-Aware Metric

Let \mathbf{X} be an image set with N training samples $\{\mathbf{x}_1, \dots, \mathbf{x}_N\}$ and \mathbf{L} be the ground truth label set $\{l_1, \dots, l_N\}$. Deep metric learning methods aim at learning a mapping to transform each image \mathbf{x}_i to an embedding space, where conventional methods [18, 27] use a deterministic vector embedding \mathbf{y}_i to represent an image. They usually adopt the Euclidean distance as the distance measure:

$$D(\mathbf{x}_1, \mathbf{x}_2) = D_E(\mathbf{x}_1, \mathbf{x}_2) = \|\mathbf{y}_1 - \mathbf{y}_2\|_2, \quad (1)$$

where $\|\cdot\|_2$ denotes the L2-norm. They then impose various constraints on the pairwise distances to enlarge interclass distances and reduce intraclass distances.

Conventional DML methods only represent the semantic information in the embedding space, ignoring the possible

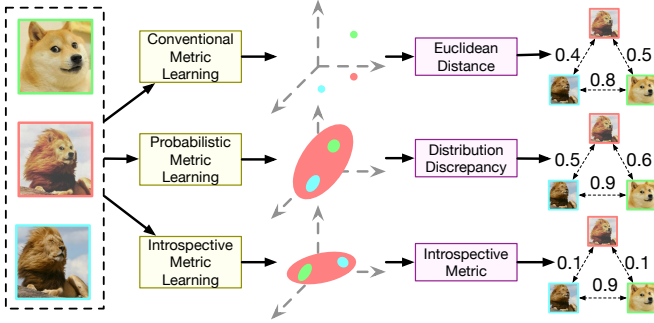


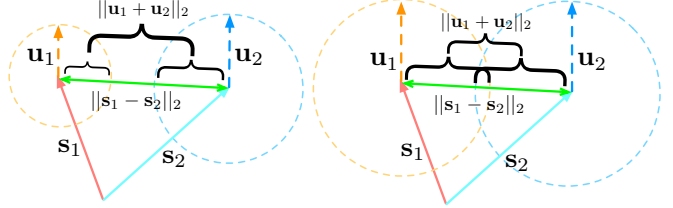
Figure 2. Comparisons between different similarity metrics. Conventional metric learning and probabilistic metric learning both produce a discriminative distance for a pair of images regardless of the uncertainty level. Our introspective similarity metric weakens the semantic discrepancies for uncertain pairs.

uncertainty in images. However, the semantic uncertainty widely exists resulting from low resolution, blur, occlusion, or semantic ambiguity of images, which motivates probabilistic embedding learning approaches [7, 32] to model images as statistical distributions \mathbf{Y} in the embedding space. They further use the distribution variance σ to measure the uncertainty of the image in the embedding space. A widely used method is to employ a Gaussian distribution to describe an image [32], *i.e.*, $\mathbf{Y} \sim N(\mu, \sigma)$, where they use a deep network to learn two vectors μ and σ as the mean and variance of the distribution, respectively, assuming each dimension is independent. They employ distribution divergences [16, 63] or Monte-Carlo-sampling-based [32] distances as the similarity metric. For instance, Hershey *et al.* [16] adopted the KL-divergence to measure the discrepancy of two Gaussian distributions \mathbf{Y}_1 and \mathbf{Y}_2 :

$$D_{KL} = -\frac{1}{2} \sum_{k=1}^d \left[\log \frac{\sigma_{1,k}^2}{\sigma_{2,k}^2} - \frac{\sigma_{1,k}^2}{\sigma_{2,k}^2} - \frac{(\mu_{1,k} - \mu_{2,k})^2}{\sigma_{2,k}^2} + 1 \right], \quad (2)$$

where d denotes the dimension of the Gaussian distributions, $\mathbf{Y}_1 \sim N(\mu_1, \sigma_1)$, and $\mathbf{Y}_2 \sim N(\mu_2, \sigma_2)$, and $\sigma_{1,k}$ denotes the k th component of σ_1 .

One can find that for two distributions with the same mean, their discrepancy solely depends on the ratio of the variance. The discrepancy still varies greatly when the variance of one image is large, *i.e.*, of large uncertainty. In other words, it still provides confident judgments about the similarity even when uncertain. However, we argue that a good similarity metric should weaken the semantic discrepancies for uncertain image pairs to allow confusion during training, which has been proven to be useful in knowledge distillation [17]. This avoids the false pulling of ambiguous pairs to improve the generalization of the learned model. Figure 2 presents the comparisons between different metrics.



Certain: $\beta(\mathbf{x}_1, \mathbf{x}_2) < \alpha(\mathbf{x}_1, \mathbf{x}_2)$ Uncertain: $\beta(\mathbf{x}_1, \mathbf{x}_2) > \alpha(\mathbf{x}_1, \mathbf{x}_2)$

Figure 3. Illustration of the proposed uncertain-aware comparison of images. We consider both the semantic discrepancy $\alpha(\mathbf{x}_1, \mathbf{x}_2) = \|\mathbf{s}_1 - \mathbf{s}_2\|_2$ and the uncertainty level $\beta(\mathbf{x}_1, \mathbf{x}_2) = \|\mathbf{u}_1 + \mathbf{u}_2\|_2$ to compute the similarity. We deem it uncertain to distinguish a pair when $\beta(\mathbf{x}_1, \mathbf{x}_2) > \alpha(\mathbf{x}_1, \mathbf{x}_2)$. We only demonstrate the case when \mathbf{u}_1 and \mathbf{u}_2 align with each other for simplicity. Practically, we use $\|\mathbf{u}_1 + \mathbf{u}_2\|_2$ instead of $\|\mathbf{u}_1\|_2 + \|\mathbf{u}_2\|_2$ to facilitate more capacity.

3.2. Introspective Similarity Metric

To facilitate an uncertainty-aware similarity metric, we first need to model the uncertainty in images. Different from existing probabilistic deep embedding learning methods to model images as distributions, we propose to represent an image using a semantic embedding \mathbf{s} and an uncertainty embedding \mathbf{u} , *i.e.*, $\mathbf{y} = \{\mathbf{s}, \mathbf{u}\}$. The semantic embedding \mathbf{s} describes the semantic characteristics of an image while the uncertainty embedding \mathbf{u} models the ambiguity.

For comparing two images \mathbf{x}_1 and \mathbf{x}_2 , we define the semantic distance as $\alpha(\mathbf{x}_1, \mathbf{x}_2) = \|\mathbf{s}_1 - \mathbf{s}_2\|_2$ similar to conventional DML methods but further compute a similarity uncertainty as $\beta(\mathbf{x}_1, \mathbf{x}_2) = \|\mathbf{u}_1 + \mathbf{u}_2\|_2$. Note that we add the vectors of the uncertainty embeddings before computing the norm instead of directly adding their norms. The reason is that the uncertainty should depend on both concerning images. For example, it might be difficult to differentiate an image from an elephant, but it can be affirmatively distinguished from a person.

When determining the semantic similarity between two images, an introspective metric needs to consider both the semantic distance and the similarity uncertainty. When not certain enough, the metric refuses to distinguish semantic discrepancies, as illustrated in Figure 3. Formally, we consider it reckless to identify the semantic discrepancy between \mathbf{x}_1 and \mathbf{x}_2 when:

$$\beta(\mathbf{x}_1, \mathbf{x}_2) + \gamma \geq \alpha(\mathbf{x}_1, \mathbf{x}_2), \quad (3)$$

where $\gamma > 0$ is the introspective bias indicating the introspective degree of the metric. The positive value of γ represents that the metric is still suspicious even if the image representation model provides no uncertainty. We then define a strict introspective similarity metric as:

$$\tilde{D}_{IN}(\mathbf{x}_1, \mathbf{x}_2) = \alpha(\mathbf{x}_1, \mathbf{x}_2) \cdot I(\alpha(\mathbf{x}_1, \mathbf{x}_2) - \beta(\mathbf{x}_1, \mathbf{x}_2) - \gamma), \quad (4)$$

where $I(x)$ is an indicator function which outputs 1 if $x > 0$ and 0 otherwise.

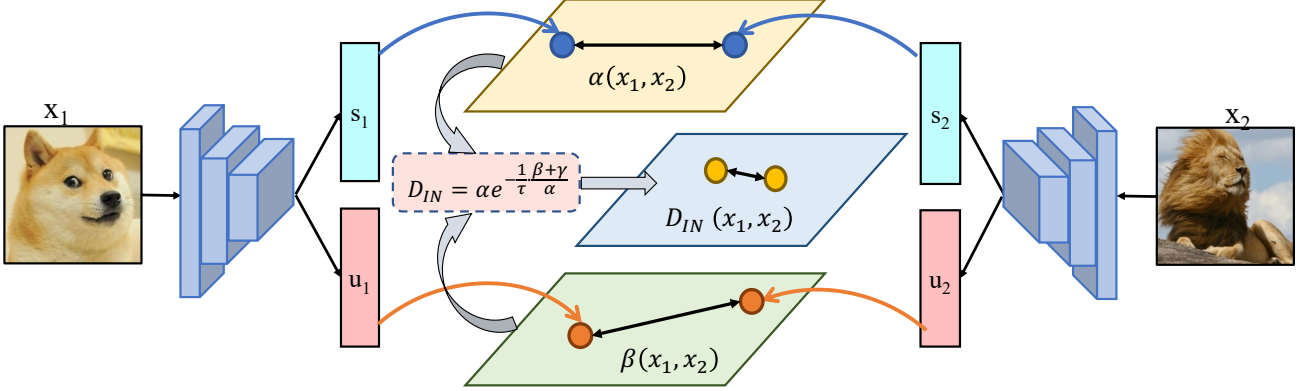


Figure 4. An illustration of the proposed IDML framework. We employ a convolutional neural network to represent each image by a semantic embedding and an uncertainty embedding. We then use the distance between semantic embeddings as the semantic discrepancy and add the uncertainty embeddings for uncertainty measure. The introspective similarity metric then uses the uncertainty level to weaken the semantic discrepancy to make a discreet similarity judgment.

However, the use of an indicator function is too strict and hard to optimize during training. We instead compare the semantic distance and the similarity uncertainty to define the relative uncertainty of two images:

$$\text{r_conf}(\mathbf{x}_1, \mathbf{x}_2) = \frac{\beta(\mathbf{x}_1, \mathbf{x}_2) + \gamma}{\alpha(\mathbf{x}_1, \mathbf{x}_2)}. \quad (5)$$

Note that the relative uncertainty is constantly positive. We then use it to soften the semantic discrepancy to obtain our introspective similarity metric:

$$D_{IN}(\mathbf{x}_1, \mathbf{x}_2) = \alpha(\mathbf{x}_1, \mathbf{x}_2) \cdot e^{(-\frac{1}{\tau} \text{r_conf}(\mathbf{x}_1, \mathbf{x}_2))}, \quad (6)$$

$\tau > 0$ is a pre-defined hyperparameter to control the weakening degree. Note that the proposed introspective similarity metric does not satisfy the triangular equation and thus is not a mathematically strict metric. We follow existing work [31, 64] to still refer to it as a metric.

Intuitively, the proposed introspectively metric considers both the semantic distance and the similarity uncertainty between two images to conduct the final semantic discrepancies. It generally produces a smaller distance for two images due to the awareness of the uncertainty. Given two pairs of images with the same semantic distance, the introspective metric distinguishes better for the pair with a smaller similarity uncertainty. Also, when the uncertainty of two images outweighs the semantic distance to a great extent, the introspective metric simply outputs a near-zero semantic distance avoiding unnecessary influence on the network.

3.3. Introspective Deep Metric Learning

We demonstrate how to apply the proposed introspective metric to existing methods and present the overall framework of IDML, as illustrated in Figure 4.

The semantic uncertainty naturally exists in images, yet it is hard to accurately describe the uncertainty for

each image. Moreover, many data augmentation methods [10, 66, 69] in the literature expand the training data by generating synthetic images, which are known to possess multiple concepts. Specifically, we employ the data mixing strategy [66, 69] to demonstrate the advantage of our framework to deal with data with large uncertainty.

Although data uncertainty naturally exists in original images, we utilize the Mixup [69] method to generate images with larger uncertainty to prove that our framework is capable of processing ambiguous data more effectively and achieving better performances. Specifically, we mix the original images \mathbf{x}_1 and \mathbf{x}_2 to obtain $\mathbf{x}_m = \lambda \cdot \mathbf{x}_1 + (1 - \lambda) \cdot \mathbf{x}_2$. However, different from the Mixup method [69] which combines the labels of two images by $l_m = \lambda \cdot l_1 + (1 - \lambda) \cdot l_2$, we treat l_m as a set which simultaneously includes l_1 and l_2 , noted as $l_m = \{l_1, l_2\}$. On such condition, we define $l_i = l_j$ if $l_i \cap l_j \neq \emptyset$ and $l_i \neq l_j$ otherwise. We adopt the convolutional network to extract the feature embeddings of both original images and mixed images $\mathbf{y}_i = f(\mathbf{x}_i) = \{\mathbf{s}_i, \mathbf{u}_i\}$, where \mathbf{s}_i and \mathbf{u}_i denote the semantic feature embedding and the uncertainty feature embedding of \mathbf{x}_i , respectively.

The similarity computation of paired samples follows our introspective similarity metric. In addition, our introspective similarity is compatible with a variety of loss formulations. For example, we can employ the margin loss with the distance-weighted sampling strategy [58] to optimize the pairwise distances:

$$J_m(\mathbf{y}, \mathbf{L}) = \sum_{l_i=l_j} [D_{IN}(\mathbf{x}_i, \mathbf{x}_j) - \xi]_+ - \sum_{l_i \neq l_j} I(p(D_{IN}(\mathbf{x}_i, \mathbf{x}_j))) [\omega - D_{IN}(\mathbf{x}_i, \mathbf{x}_j)]_+, \quad (7)$$

where $D_{IN}(\mathbf{x}_i, \mathbf{x}_j)$ follows (6), the random variable $I(p)$ has a probability of p to be 1 and 0 otherwise, $p(d) = \min(\phi, d^{2-n} [1 - \frac{1}{4}d^2]^{\frac{3-n}{2}})$, $[\cdot]_+ = \max(\cdot, 0)$, ξ and ω are two pre-defined margins, and ϕ is a positive constant.

In addition, proxy-based losses such as the softmax loss [8, 45] fits our similarity metric as well. It should be noted that different from the Euclidean distance, various proxy-based losses compute the cosine similarity $C(\mathbf{x}_i, \mathbf{p}_j)$ between an image \mathbf{x}_i and a class-level representative \mathbf{p}_j . Therefore, we conduct the confidence decay of the semantic similarity in another way:

$$C_{IN}(\mathbf{x}_i, \mathbf{p}_j) = 1 - (1 - C(\mathbf{x}_i, \mathbf{p}_j)) \cdot e^{(-\frac{1}{\tau} \text{r.conf}(\mathbf{x}_i, \mathbf{p}_j))}, \quad (8)$$

where $\text{r.conf}(\mathbf{x}_i, \mathbf{p}_j)$ denotes the relative uncertainty between the image and the representative, and we provide the softmax loss based on our similarity metric:

$$J_s(\mathbf{y}, \mathbf{L}) = \frac{1}{N} \sum_{i=1}^N \left(-\log \frac{\sum_{l_{\mathbf{p}_j=l_i}} e^{C_{IN}(\mathbf{x}_i, \mathbf{p}_j)}}{\sum_{l_{\mathbf{p}_j \neq l_i}} e^{C_{IN}(\mathbf{x}_i, \mathbf{p}_j)}} \right), \quad (9)$$

where $l_{\mathbf{p}_j}$ is the category of the class representative \mathbf{p}_j .

For inference, we directly use the Euclidean distance between semantic embeddings as the similarity metric and can optionally use the uncertainty embedding to indicate the uncertainty level.

3.4. Gradient Analysis

We provide a gradient analysis to demonstrate the effect of our introspective similarity metric on the learning of semantic embeddings. Intuitively, our proposed similarity metric results in reduced semantic discrepancies to impose fewer influences for uncertain samples. Therefore, we present a detailed gradient analysis of the parameters of the semantic embedding layer W^t with the Euclidean-distance-based methods for example. Firstly, we formulate the back-propagation process in the t -th iteration as follows:

$$\frac{\partial J}{\partial W^t} = \frac{\partial J}{\partial \mathbf{S}} \cdot \frac{\partial \mathbf{S}}{\partial W^t} = \frac{\partial J}{\partial D_{IN}} \cdot \frac{\partial D_{IN}}{\partial \mathbf{S}} \cdot \frac{\partial \mathbf{S}}{\partial W^t}, \quad (10)$$

where J and \mathbf{S} denote the loss function and the semantic embeddings for simplicity. Actually, the partial term $\frac{\partial J}{\partial D_{IN}}$ depends on the form of the loss function while $\frac{\partial \mathbf{S}}{\partial W^t}$ is merely relevant to the architecture of the network. On such condition, $\frac{\partial D_{IN}}{\partial \mathbf{S}}$ contributes to the update level of the parameters, and a larger gradient undoubtedly represents a larger update. Next, we formulate the above gradient based on a paired samples $\{\mathbf{y}_1 = (\mathbf{s}_1, \mathbf{u}_1), \mathbf{y}_2 = (\mathbf{s}_2, \mathbf{u}_2)\}$, which is as follows: (D_{IN} is the same as (6) and we set $\tau = 1$ and $\gamma = 0$ for simplicity.)

$$\begin{aligned} H(\mathbf{u}_1, \mathbf{u}_2) &= \frac{\partial D_{IN}(\mathbf{x}_1, \mathbf{x}_2)}{\partial \mathbf{s}_1} \\ &= \frac{\partial \|\mathbf{s}_1 - \mathbf{s}_2\|_2}{\partial \mathbf{s}_1} \cdot e^{-\frac{\|\mathbf{u}_1 + \mathbf{u}_2\|_2}{\|\mathbf{s}_1 - \mathbf{s}_2\|_2}} \cdot \left(1 + \frac{\|\mathbf{u}_1 + \mathbf{u}_2\|_2}{\|\mathbf{s}_1 - \mathbf{s}_2\|_2}\right) \end{aligned} \quad (11)$$

where $H(\mathbf{u}_1, \mathbf{u}_2)$ is a function of $\{\mathbf{u}_1, \mathbf{u}_2\}$ if the semantic feature embeddings $\{\mathbf{s}_1, \mathbf{s}_2\}$ are fixed, $\frac{\partial \|\mathbf{s}_1 - \mathbf{s}_2\|_2}{\partial \mathbf{s}_1}$ denotes

the gradient for the original Euclidean distance form, and $e^{-\frac{\|\mathbf{u}_1 + \mathbf{u}_2\|_2}{\|\mathbf{s}_1 - \mathbf{s}_2\|_2}} \cdot \left(1 + \frac{\|\mathbf{u}_1 + \mathbf{u}_2\|_2}{\|\mathbf{s}_1 - \mathbf{s}_2\|_2}\right)$ connects with the commonly used monotone decreasing function $g(x) = e^{-x} \cdot (1 + x)$ when $x > 0$, which remains decreasing when $\mathbf{u}_1 > 0$.

Therefore, $H(\mathbf{u}_1, \mathbf{u}_2)$ decreases when the length of the uncertainty embedding \mathbf{u}_1 increases. It indicates that images with more uncertainty result in smaller gradients, thus imposing fewer influences on the network. Specially, when $\|\mathbf{u}_1 + \mathbf{u}_2\|_2 = 0$, denoting the absolute certainty of samples, $H(\mathbf{u}_1, \mathbf{u}_2) = \frac{\partial \|\mathbf{s}_1 - \mathbf{s}_2\|_2}{\partial \mathbf{s}_1}$, turning back to the form of the original Euclidean gradient. It denotes that our similarity metric maintains the original judgment for certain samples.

4. Experiments

In this section, we conducted various experiments to evaluate the performance of our IDML framework on image retrieval. We show that employing the proposed introspective similarity metric consistently improves the performance of existing deep metric learning and data mixing methods. We also provide in-depth analyses of the effectiveness of our framework.

4.1. Settings

We first evaluated our framework under the conventional deep metric learning setting [43, 55] and conducted experiments on three widely-used datasets: CUB-200-2011 [51], Cars196 [24], and Stanford Online Products [43]. We provide the detailed dataset splits in the supplementary material. We adopted the ImageNet [37] pretrained ResNet-50 [15] as the backbone and two randomly initialized fully connected layers to obtain the semantic embedding and uncertainty embedding, respectively. We set the embedding size to 512 for the main experiments. The training images were first resized to 256×256 and then augmented with random cropping to 224×224 as well as random horizontal flipping with the probability of 50%. We employed Mixup [69] for our framework to generate images with large uncertainty for training. We fixed the batch size to 120 and used the AdamW optimizer with the learning rate of 10^{-5} . We set $\gamma = 3$ for Cars196 and $\gamma = 0$ for the other datasets and fixed $\epsilon = 5$ for all the datasets during training. We adopted the original similarity metric without our uncertainty-aware term for testing. The reported evaluation metrics include Recall@Ks, normalized mutual information (NMI), R-Precision (RP), and Mean Average Precision at R (M@R). See Musgrave *et al.* [28] for more details.

4.2. Dataset

For image retrieval and clustering, we followed existing DML methods [22, 43, 55, 72] to conduct experiments on the CUB-200-2011 [51], Cars196 [24], and Stanford Online Products [43]. CUB-200-2011 contains 11,788 images

Table 1. Experimental results (%) on the CUB-200-2011, Cars196, and Stanford Online Products datasets compared with state-of-the-art methods. * denotes our reproduced results under the same settings.

Method	Setting	CUB-200-2011					Cars196					Stanford Online Products				
		R@1	R@2	NMI	RP	M@R	R@1	R@2	NMI	RP	M@R	R@1	R@10	NMI	RP	M@R
ABE-8 [23]	512G	60.6	71.5	-	-	-	85.2	90.5	-	-	-	76.3	88.4	-	-	-
Ranked [56]	1536BN	61.3	72.7	66.1	-	-	82.1	89.3	71.8	-	-	79.8	91.3	90.4	-	-
DREML [59]	9216R	63.9	75.0	67.8	-	-	86.0	91.7	76.4	-	-	-	-	-	-	-
SoftTriple [33]	512BN	65.4	76.4	69.3	-	-	84.5	90.7	70.1	-	-	78.3	90.3	92.0	-	-
D & C [38]	128R	65.9	76.6	69.6	-	-	84.6	90.7	70.3	-	-	75.9	88.4	90.2	-	-
MIC [34]	128R	66.1	76.8	69.7	-	-	82.6	89.1	68.4	-	-	77.2	89.4	90.0	-	-
RankMI [20]	128R	66.7	77.2	71.3	-	-	83.3	89.8	69.4	-	-	74.3	87.9	90.5	-	-
CircleLoss [45]	512R	66.7	77.4	-	-	-	83.4	89.8	-	-	-	78.3	90.5	-	-	-
PADS [35]	128BN	67.3	78.0	69.9	-	-	83.5	89.7	68.8	-	-	76.5	89.0	89.9	-	-
DIML [71]	512R	68.2	-	-	37.9	26.9	87.0	-	-	39.0	29.4	79.3	-	-	46.4	43.2
DCML [76]	512R	68.4	77.9	71.8	-	-	85.2	91.8	73.9	-	-	79.8	90.8	90.8	-	-
DRML [77]	512BN	68.7	78.6	69.3	-	-	86.9	92.1	72.1	-	-	79.9	90.7	90.1	-	-
ProxyNCA++ [47]	512R	69.0	79.8	73.9	-	-	86.5	92.5	73.8	-	-	80.7	92.0	-	-	-
DiVA [26]	512R	69.2	79.3	71.4	-	-	87.6	92.9	72.2	-	-	79.6	91.2	90.6	-	-
NIR [36]	512R	70.5	80.6	72.5	-	-	89.1	93.4	75.0	-	-	80.7	91.5	90.9	-	-
Triplet-SH* [39]	512R	63.6	75.5	67.9	35.1	24.0	70.8	81.7	64.8	31.7	21.1	76.5	89.1	89.7	51.3	48.4
IDML-TSH	512R	65.3	76.5	69.5	36.2	25.0	73.7	84.0	67.3	33.8	24.1	77.4	89.4	90.1	51.9	49.0
ProxyNCA* [27]	512R	64.6	75.6	69.1	35.5	24.7	82.6	89.0	66.4	33.5	23.5	77.0	89.1	89.5	51.9	49.0
IDML-PN	512R	66.0	76.4	70.1	36.5	25.4	85.5	91.3	69.0	36.1	26.4	78.3	90.1	89.9	53.0	49.9
FastAP* [2]	512R	65.1	75.4	68.5	35.9	24.1	81.6	88.5	68.8	35.1	25.2	75.9	89.2	89.7	50.1	46.8
IDML-FAP	512R	66.4	76.4	69.7	36.7	25.5	83.9	89.9	71.9	36.5	26.7	76.8	89.7	90.9	50.9	47.9
Contrastive* [18]	512R	65.6	76.5	68.9	36.5	24.7	82.7	89.6	69.5	35.8	25.7	76.4	88.5	88.9	50.9	47.9
IDML-Con	512R	67.2	77.6	71.3	37.5	25.7	85.5	91.5	72.5	38.8	29.0	77.3	89.7	90.0	51.7	48.5
Margin-DW* [58]	512R	65.9	77.0	69.5	36.0	24.9	82.6	88.7	69.3	36.4	26.5	78.5	89.9	90.1	53.4	50.2
IDML-MDW	512R	67.9	78.3	72.1	37.2	26.1	86.1	91.7	73.0	39.2	29.7	79.4	90.6	91.0	53.7	50.4
Multi-Sim* [55]	512R	67.3	78.2	72.7	36.6	25.5	83.3	90.9	72.2	37.4	27.4	78.1	90.0	89.9	52.9	49.9
IDML-MS	512R	69.0	79.5	73.5	38.5	27.2	86.3	92.2	74.1	40.0	30.8	79.7	91.4	91.2	53.7	50.9
ProxyAnchor* [22]	512R	69.0	79.4	72.3	38.5	27.5	87.3	92.7	75.7	40.9	31.8	79.5	91.1	91.0	53.7	50.5
IDML-PA	512R	70.7	80.2	73.5	39.3	28.4	90.6	94.5	76.9	42.6	33.8	81.5	92.7	92.3	54.8	51.3

of 200 bird species. We used the first 100 species with 5,864 images for training and the rest 100 species with 5,924 images are for testing. Cars196 includes 16,183 images of 196 car models. We used the first 96 classes with 8,054 images for training and the rest 98 classes with 8,131 images for testing. Stanford Online Products is relatively large and contains 120,053 images of 22,634 products. We used the first 11,318 products with 59,551 images in the training set and the rest 11,318 products with 60,502 images for testing.

4.3. Main Results

We evaluated the proposed IDML framework under the conventional deep metric learning setting and compared it

with state-of-the-art methods. To demonstrate the versatility of our framework, we applied the introspective similarity metric to various loss functions, including the triplet loss with the semi-hard sampling (Triplet-SH) [39], the ProxyNCA loss [27], the FastAP loss [2], the contrastive loss [18], the margin loss with the distance-weighted sampling (Margin-DW) [58], the multi-similarity loss (Multi-Sim) [55], and the ProxyAnchor loss [22].

Table 1 shows the experimental results on the CUB-200-2011 [51], Cars196 [24], and Stanford Online Products [43] datasets. The n-BN/R denotes the model setting where n is the embedding size and BN, R represents BN-Incertion [19] and ResNet-50 [15], respectively. The bold numbers high-

Table 2. Analysis of different components of IDML on the CUB-200-2011, Cars196, and Stanford Online Products datasets.

Method	CUB-200-2011				Cars196				Stanford Online Products			
	R@1	NMI	RP	M@R	R@1	NMI	RP	M@R	R@1	NMI	RP	M@R
Margin-DW [58]	65.9	69.5	36.0	24.9	82.6	69.3	36.4	26.5	78.5	90.1	53.4	50.2
Mixup-MDW	67.1	71.6	36.7	25.5	84.7	72.4	38.0	28.0	79.1	90.5	53.6	50.4
ISM-MDW	67.0	71.4	36.9	25.7	84.4	71.9	37.9	28.1	78.9	90.4	53.6	50.3
PEL-MDW [32]	63.3	67.1	34.6	24.2	80.4	67.1	34.8	25.5	76.4	88.7	51.2	48.7
PEL-Mixup-MDW	64.5	68.6	35.3	24.7	82.3	68.9	35.9	26.1	77.2	89.4	52.1	49.3
IDML-MDW	67.9	72.1	37.2	26.1	86.1	73.0	39.2	29.7	79.4	91.0	53.7	50.4
ProxyAnchor [22]	69.0	72.3	38.5	27.5	87.3	75.7	40.9	31.8	79.5	91.0	53.7	50.5
Mixup-PA	69.8	73.0	39.1	28.1	88.5	75.8	41.0	32.1	80.6	91.8	54.4	50.7
ISM-PA	69.5	73.1	38.9	28.0	88.8	75.8	41.2	32.2	80.3	91.8	54.3	50.9
PEL-PA [32]	64.9	67.1	34.5	23.7	83.4	66.4	34.4	24.9	76.8	89.7	51.8	48.7
PEL-Mixup-PA	65.7	68.0	35.6	24.7	84.5	66.6	34.6	25.1	77.9	90.5	52.6	49.9
IDML-PA	70.7	73.5	39.3	28.4	90.6	76.9	42.6	33.8	81.5	92.3	54.8	51.3

Table 3. Experimental results with various forms of uncertain data.

Method	CUB-200-2011				Cars196				Stanford Online Products			
	R@1	NMI	RP	M@R	R@1	NMI	RP	M@R	R@1	NMI	RP	M@R
Baseline	69.0	72.3	38.5	27.5	87.3	75.7	40.9	31.8	79.5	91.0	53.7	50.5
Baseline + ISM	69.5	73.1	38.9	28.0	88.8	75.8	41.2	32.2	80.3	91.8	54.3	50.9
Low-res (200×200)	67.4	71.3	37.7	26.2	87.0	75.3	40.8	31.2	78.7	90.0	52.6	49.1
Low-res + ISM	68.9	71.9	38.2	27.4	89.0	76.2	41.3	32.5	79.3	90.9	53.4	50.4
Blur (p=0.5)	69.0	72.4	38.5	27.7	88.2	75.8	41.1	32.0	79.7	91.0	53.9	50.5
Blur + ISM	69.2	72.5	38.6	27.7	89.6	76.4	41.8	32.8	79.7	91.1	53.9	50.3
Occlusion (p=0.5)	69.3	72.4	38.6	27.9	87.9	75.7	41.1	31.8	80.2	91.2	54.2	50.7
Occlusion + ISM	69.6	72.8	38.8	28.0	89.2	76.4	41.5	32.6	80.6	91.7	54.6	50.9
Mixup	69.8	73.0	39.1	28.1	88.5	75.8	41.0	32.1	80.6	91.8	54.4	50.7
Mixup + ISM	70.7	73.5	39.3	28.4	90.6	76.9	42.6	33.8	81.5	92.3	54.8	51.3

light the improvement of our framework compared with the original method, and red numbers indicate the best results. We observe that our framework achieves a constant performance boost to all the associated methods. Furthermore, we attain state-of-the-art performance on all three datasets by applying our framework to the ProxyAnchor loss, which surpasses the original performance by 3.3% at Recall@1 and 2.0% at M@R on the Cars196 dataset, respectively. This is because the proposed similarity metric is aware of the data uncertainty in images so that the uncertain samples only provide limited training signals.

4.4. Analysis

Ablation Study of Different Components: We conducted experiments with the margin loss and ProxyAnchor loss to analyze the effect of different components of our framework, as shown in Table 2. We first applied Mixup to the baseline method (Mixup-MDW) without using our introspective similarity metric and then only employed the

proposed metric without mixup (ISM-MDW). We see that the Mixup method and the proposed ISM can independently boost the performances of the baseline method. Our IDML framework further improves the performance by combining Mixup and our ISM. Furthermore, we reproduced the probabilistic embedding learning (PEL) framework [32] on each loss (PEL-MDW) and also equipped it with Mixup (PEL-Mixup-MDW) for fair comparisons with our framework. We observe that it achieves lower performance than the baseline method, and further using Mixup improves the performance. The performance drop might result from the compromise of discriminativeness when representing images as distributions. Differently, IDML uses an uncertainty embedding to model the uncertainty which does not affect the discriminativeness of the semantic embedding.

Uncertainty of Other Forms: In addition to Mixup, we further conducted experiments when training with lowered-resolution, blurred, and occluded images, as shown in Table 3. Though certain augmentations (*e.g.*, low-resolution)

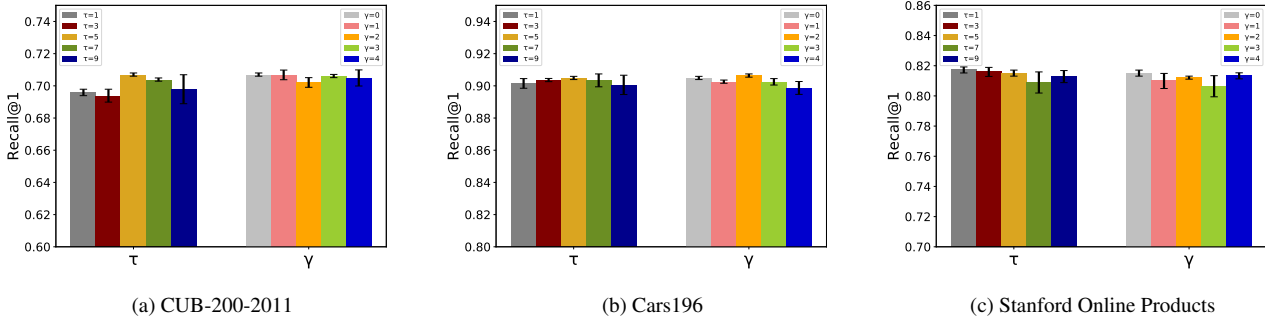


Figure 5. Impact of metric parameters on the CUB-200-2011, Cars196 and Stanford Online Products datasets.

Table 4. Effect of different metric formulations during training.

Dataset	Training Metric	R@1	NMI	RP	M@R
CUB-200-2011	Euclidean	69.0	72.3	38.5	27.5
	ISM-Dis (13)	69.2	72.0	38.7	28.1
	ISM-Sim (12)	70.7	73.5	39.3	28.4
Cars196	Euclidean	87.3	75.7	40.9	31.8
	ISM-Dis (13)	89.4	75.4	41.6	32.5
	ISM-Sim (12)	90.6	76.9	42.6	33.8
SOP	Euclidean	79.5	91.0	53.7	50.5
	ISM-Dis (13)	80.2	91.3	54.0	50.6
	ISM-Sim (12)	81.5	92.3	54.8	51.3

Table 5. Effect of different metric formulations during testing.

Dataset	Testing Metric	R@1	NMI	RP	M@R
CUB-200-2011	Euclidean (baseline)	69.0	72.3	38.5	27.5
	ISM (IDML)	69.8	73.1	39.0	27.8
	Euclidean (IDML)	70.7	73.5	39.3	28.4
Cars196	Euclidean (baseline)	87.3	75.7	40.9	31.8
	ISM (IDML)	89.9	76.2	42.3	33.3
	Euclidean (IDML)	90.6	76.9	42.6	33.8
SOP	Euclidean (baseline)	79.5	91.0	53.7	50.5
	ISM (IDML)	80.7	92.1	54.2	50.8
	Euclidean (IDML)	81.5	92.3	54.8	51.3

reduce the performance of the baseline, further applying our ISM consistently attains better results than training without these augmentations. For example, adopting the low-resolution augmentation achieves 67.4% at Recall@1 on the CUB-200-211 dataset, which is 1.6% lower than the baseline, while further applying ISM improves the performance by 1.5% and is close to the original baseline method. This verifies the effectiveness of our method to deal with various forms of uncertain data.

Effect of the Hyper-parameters γ and τ : γ determines the introspective bias and τ controls the weakening degree in our introspective similarity metric. They jointly affect the final performance of our framework. We experimentally evaluated their impacts as demonstrated in Figure 5. We first fixed γ to 0 and set τ to 1, 3, 5, 7, 9. We see that our framework achieves the best recall@1 when $\tau = 5$ for both datasets, indicating the favor of a modest weakening degree. In addition, we fixed $\tau = 5$ and set γ to 0, 1, 2, 3, 4 for training. The experimental results vary on the two datasets. Specifically, our framework achieves the best performance when $\gamma = 0$ on the CUB-200-2011 dataset while $\gamma = 3$ on the Cars196 dataset. This indicates that the metric is more discreet when comparing images on the Cars196 dataset.

Effect of the Metric Formulation during Training: When uncertain, the proposed metric tends to treat the pair similarly since we think an uncertain metric should not be able to differentiate all pairs. The proposed introspective

similarity metric (ISM-Sim) based on the cosine similarity is defined as follows:

$$C_{IN}(\mathbf{x}_i, \mathbf{p}_j) = 1 - (1 - C(\mathbf{x}_i, \mathbf{p}_j)) \cdot e^{(-\frac{1}{\tau} r_{\text{conf}}(\mathbf{x}_i, \mathbf{p}_j))}. \quad (12)$$

Alternatively, we may also weaken the similarity judgment by encouraging the metric to output large distances to all uncertain pairs. As a comparison, we additionally modified the metric to treat each ambiguous pair dissimilar (ISM-Dis) as follows:

$$C_{IN}(\mathbf{x}_i, \mathbf{p}_j) = C(\mathbf{x}_i, \mathbf{p}_j) \cdot e^{(-\frac{1}{\tau} r_{\text{conf}}(\mathbf{x}_i, \mathbf{p}_j))}. \quad (13)$$

We conducted experiments on the CUB-200-2011 and Cars196 datasets to test the performances of using different metric formulations for training in Table 4. We observe that treating each ambiguous pair dissimilar performs worse than the original metric. This verifies our motivation for using uncertainty to weaken the semantic discrepancy.

Effect of the Metric Formulation during Testing: During testing, we adopt the original similarity metric without our uncertainty-aware term. As an alternative, we conducted an experiment using the introspective similarity metric (ISM) during testing, as shown in Table 5. We observe a decrease in performance when using ISM during testing, indicating a harmful effect of using uncertainty to weaken the similarity discrepancy during inference. This is reasonable since providing a clear and confident similarity judgment is more beneficial to discriminative tasks.

Table 6. Analysis of the batch size (BS) on the CUB-200-2011, Cars196, and Stanford Online Products datasets.

BS	CUB-200-2011		Cars196		SOP	
	R@1	NMI	R@1	NMI	R@1	NMI
40	66.3	70.6	88.2	74.1	78.1	89.5
60	67.1	71.3	88.9	75.3	79.9	91.3
80	68.5	72.0	89.6	75.6	80.5	91.6
100	69.6	72.5	90.0	76.3	81.2	92.1
120	70.7	73.5	90.6	76.9	81.5	92.3
140	70.5	73.2	90.5	77.2	81.6	92.2
160	70.7	73.3	90.7	76.8	81.3	92.3
180	70.7	73.6	90.5	77.5	81.3	92.1

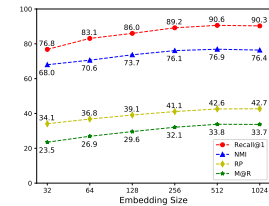


Figure 6. Effect of the embedding size on Cars196.

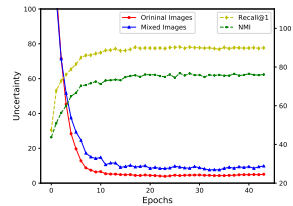


Figure 7. Uncertainty trend during training on Cars196.

Effect of the Batch Size: We conducted experiments to investigate the influence of different batch sizes during training. Specifically, we set the batch size from 40 to 180, as shown in Table 6. We observe a relatively consistent performance improvement as the batch size increases. This is because larger batch sizes enable richer relation mining among data. Still, we see that the performance plateaus and even decreases when the batch sizes exceed 120. Therefore, we set the batch size to 120 for the main experiments for a better balance of performance and computation.

Effect of the Embedding Size: We provided the experimental results with different embedding sizes on the Cars196 dataset in Figure 6. We observe that the performance already surpasses existing methods when the embedding size reaches 256, indicating the superiority of the proposed IDML framework.

Uncertainty Trend during Training: To demonstrate that our IDML framework properly handles mixed images with high uncertainty, we visualize the trend of uncertainty level for both original images and mixed images during training, as shown in Figure 7. We define the uncertainty level of an image to be the L2-norm of its uncertainty embedding. We see that the uncertainty decreases for both original and mixed images as the training proceeds and becomes stable as the model converges. We also observe that the uncertainty level for mixed images is larger than that of original images. This verifies that our framework can indeed learn the uncertainty in images.

Qualitative Analysis of the Learning Process: We provide a t-SNE [48] visualized analysis of how embeddings

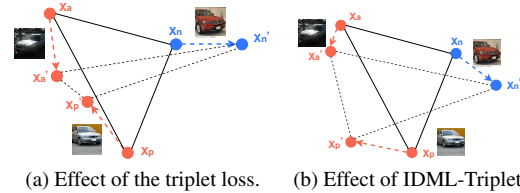


Figure 8. T-SNE [48] analysis of one-step updating of the embeddings.

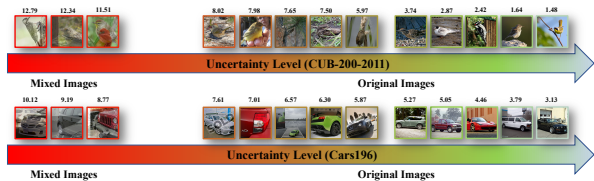


Figure 9. Uncertainty levels produced by the proposed IDML framework on the test split of CUB-200-2011 and Cars196.

are learned using a toy example on the Cars196 dataset in Figure 8. We visualized the embeddings before and after updating the model with one gradient step. For a dark (and ambiguous) image x_α , the original method pulls it quite closer to the positive sample x_p , while the proposed IDML is more cautious and only slightly pulls it together due to the uncertainty to prevent the influence of possible noise.

Uncertainty Levels on the Test Split: We visualize the uncertainty levels on the test split of the CUB-200-2011 and Cars196 datasets, as shown in Figure 9. We obtain the uncertainty levels of the mixed images together with original images in the test set after the model converges. We observe that the uncertainty of mixed images is much larger than that of the original test images since the mixed images contain the information of two images. Also, we see that several original images result in relatively higher uncertainty than others because of the natural noise such as occlusion and improper directions. This further verifies that the proposed framework can successfully learn the uncertainty in images.

5. Conclusion

In this paper, we have presented an introspective deep metric learning (IDML) framework to properly process the data uncertainty for better performance. We have represented an image with a semantic embedding and an uncertainty embedding to model the semantic characteristics and the uncertainty, respectively. We have further proposed an introspective similarity metric to compute an uncertainty-aware similarity score, which weakens semantic discrepancies for uncertain images. We have performed various experiments on the widely used benchmark datasets on both image retrieval to analyze the effectiveness of the proposed framework. Experimental results have demonstrated a constant performance boost to various methods in different settings. It is interesting to apply our framework to self-supervised learning and vision transformers as future work.

References

- [1] Artem Babenko, Anton Slesarev, Alexandr Chigorin, and Victor Lempitsky. Neural codes for image retrieval. In *ECCV*, pages 584–599, 2014. 1
- [2] Fatih Cakir, Kun He, Xide Xia, Brian Kulis, and Stan Sclaroff. Deep metric learning to rank. In *CVPR*, pages 1861–1870, 2019. 2, 6
- [3] Jie Chang, Zhonghao Lan, Changmao Cheng, and Yichen Wei. Data uncertainty learning in face recognition. In *CVPR*, pages 5710–5719, 2020. 2
- [4] Ting Chen, Simon Kornblith, Mohammad Norouzi, and Geoffrey Hinton. A simple framework for contrastive learning of visual representations. In *ICML*, pages 1597–1607, 2020. 1
- [5] Xinlei Chen and Kaiming He. Exploring simple siamese representation learning. In *CVPR*, pages 15750–15758, 2021. 1
- [6] Hsin-Ping Chou, Shih-Chieh Chang, Jia-Yu Pan, Wei Wei, and Da-Cheng Juan. Remix: Rebalanced mixup. In *ECCV*, pages 95–110, 2020. 2
- [7] Sanghyuk Chun, Seong Joon Oh, Rafael Sampaio de Rezende, Yannis Kalantidis, and Diane Larlus. Probabilistic embeddings for cross-modal retrieval. In *CVPR*, pages 8415–8424, 2021. 1, 2, 3
- [8] Jiankang Deng, Jia Guo, Niannan Xue, and Stefanos Zafeiriou. Arcface: Additive angular margin loss for deep face recognition. In *CVPR*, pages 4690–4699, 2019. 1, 2, 5
- [9] Thanh-Toan Do, Toan Tran, Ian Reid, Vijay Kumar, Tuan Hoang, and Gustavo Carneiro. A theoretically sound upper bound on the triplet loss for improving the efficiency of deep distance metric learning. In *CVPR*, pages 10404–10413, 2019. 2
- [10] Yueqi Duan, Wenzhao Zheng, Xudong Lin, Jiwen Lu, and Jie Zhou. Deep adversarial metric learning. In *CVPR*, pages 2780–2789, 2018. 2, 4
- [11] Jean-Bastien Grill, Florian Strub, Florent Althé, Corentin Tallec, Pierre Richemond, Elena Buchatskaya, Carl Doersch, Bernardo Avila Pires, Zhaohan Guo, Mohammad Gheshlaghi Azar, et al. Bootstrap your own latent—a new approach to self-supervised learning. In *NeurIPS*, pages 21271–21284, 2020. 1
- [12] Senhui Guo, Jing Xu, Dapeng Chen, Chao Zhang, Xiaogang Wang, and Rui Zhao. Density-aware feature embedding for face clustering. In *CVPR*, pages 6698–6706, 2020. 1
- [13] Ben Harwood, Vijay Kumar B G, Gustavo Carneiro, Ian Reid, and Tom Drummond. Smart mining for deep metric learning. In *ICCV*, pages 2840–2848, 2017. 2
- [14] Kaiming He, Haoqi Fan, Yuxin Wu, Saining Xie, and Ross Girshick. Momentum contrast for unsupervised visual representation learning. In *CVPR*, pages 9729–9738, 2020. 1
- [15] Kaiming He, Xiangyu Zhang, Shaoqing Ren, and Jian Sun. Deep residual learning for image recognition. In *CVPR*, pages 770–778, 2016. 1, 5, 6
- [16] John R Hershey and Peder A Olsen. Approximating the kullback leibler divergence between gaussian mixture models. In *ICASSP*, pages IV–317, 2007. 1, 3
- [17] Geoffrey Hinton, Oriol Vinyals, Jeff Dean, et al. Distilling the knowledge in a neural network. In *NeurIPS*, 2015. 3
- [18] Junlin Hu, Jiwen Lu, and Yap-Peng Tan. Discriminative deep metric learning for face verification in the wild. In *CVPR*, pages 1875–1882, 2014. 2, 6
- [19] Sergey Ioffe and Christian Szegedy. Batch normalization: Accelerating deep network training by reducing internal covariate shift. In *ICLR*, pages 448–456, 2015. 6
- [20] Mete Kemertas, Leila Pishdad, Konstantinos G Derpanis, and Afsaneh Fazly. Rankmi: A mutual information maximizing ranking loss. In *CVPR*, pages 14362–14371, 2020. 6
- [21] Alex Kendall and Yarin Gal. What uncertainties do we need in bayesian deep learning for computer vision? In *NeurIPS*, pages 5574–5584, 2017. 2
- [22] Sungyeon Kim, Dongwon Kim, Minsu Cho, and Suha Kwak. Proxy anchor loss for deep metric learning. In *CVPR*, pages 3238–3247, 2020. 2, 5, 6, 7
- [23] Wonsik Kim, Bhavya Goyal, Kunal Chawla, Jungmin Lee, and Keunjoo Kwon. Attention-based ensemble for deep metric learning. In *ECCV*, pages 760–777, 2018. 6
- [24] Jonathan Krause, Michael Stark, Jia Deng, and Li Fei-Fei. 3d object representations for fine-grained categorization. In *ICCVW*, pages 554–561, 2013. 5, 6
- [25] Wanhua Li, Xiaoke Huang, Jiwen Lu, Jianjiang Feng, and Jie Zhou. Learning probabilistic ordinal embeddings for uncertainty-aware regression. In *CVPR*, pages 13896–13905, 2021. 2
- [26] Timo Milbich, Karsten Roth, Homanga Bharadhwaj, Samarth Sinha, Yoshua Bengio, Björn Ommer, and Joseph Paul Cohen. Diva: Diverse visual feature aggregation for deep metric learning. In *ECCV*, pages 590–607, 2020. 6
- [27] Yair Movshovitz-Attias, Alexander Toshev, Thomas K. Leung, Sergey Ioffe, and Saurabh Singh. No fuss distance metric learning using proxies. In *ICCV*, pages 360–368, 2017. 2, 6
- [28] Kevin Musgrave, Serge Belongie, and Ser-Nam Lim. A metric learning reality check. In *ECCV*, 2020. 5
- [29] Arvind Neelakantan, Jeevan Shankar, Alexandre Passos, and Andrew McCallum. Efficient non-parametric estimation of multiple embeddings per word in vector space. In *EMNLP*, pages 1059–1069, 2014. 2
- [30] Dai Quoc Nguyen, Dat Quoc Nguyen, Ashutosh Modi, Stefan Thater, and Manfred Pinkal. A mixture model for learning multi-sense word embeddings. *arXiv*, abs/1706.05111, 2017. 2
- [31] Hieu V Nguyen and Li Bai. Cosine similarity metric learning for face verification. In *ACCV*, pages 709–720, 2010. 4
- [32] Seong Joon Oh, Kevin P Murphy, Jiyan Pan, Joseph Roth, Florian Schroff, and Andrew C Gallagher. Modeling uncertainty with hedged instance embeddings. In *ICLR*, 2018. 1, 2, 3, 7
- [33] Qi Qian, Lei Shang, Baigui Sun, and Juhua Hu. Softtriple loss: Deep metric learning without triplet sampling. In *ICCV*, pages 6450–6458, 2019. 6
- [34] Karsten Roth, Biagio Brattoli, and Bjorn Ommer. Mic: Mining interclass characteristics for improved metric learning. In *ICCV*, pages 8000–8009, 2019. 6

- [35] Karsten Roth, Timo Milbich, and Bjorn Ommer. Pads: Policy-adapted sampling for visual similarity learning. In *CVPR*, pages 6568–6577, 2020. 6
- [36] Karsten Roth, Oriol Vinyals, and Zeynep Akata. Non-isotropy regularization for proxy-based deep metric learning. In *CVPR*, pages 7420–7430, 2022. 6
- [37] Olga Russakovsky, Jia Deng, Hao Su, Jonathan Krause, Sanjeev Satheesh, Sean Ma, Zhiheng Huang, Andrej Karpathy, Aditya Khosla, Michael Bernstein, et al. Imagenet large scale visual recognition challenge. *IJCV*, 115(3):211–252, 2015. 5
- [38] Arsiom Sanakoyeu, Vadim Tschernezki, Uta Buchler, and Bjorn Ommer. Divide and conquer the embedding space for metric learning. In *CVPR*, pages 471–480, 2019. 6
- [39] Florian Schroff, Dmitry Kalenichenko, and James Philbin. Facenet: A unified embedding for face recognition and clustering. In *CVPR*, pages 815–823, 2015. 1, 2, 6
- [40] Gary Shaw and Dimitris Manolakis. Signal processing for hyperspectral image exploitation. *SPM*, 19(1):12–16, 2002. 2
- [41] Yichun Shi and Anil K Jain. Probabilistic face embeddings. In *ICCV*, pages 6902–6911, 2019. 1, 2
- [42] Karen Simonyan and Andrew Zisserman. Very deep convolutional networks for large-scale image recognition. *arXiv*, abs/1409.1556, 2014. 1
- [43] Hyun Oh Song, Yu Xiang, Stefanie Jegelka, and Silvio Savarese. Deep metric learning via lifted structured feature embedding. In *CVPR*, pages 4004–4012, 2016. 1, 2, 5, 6
- [44] Jennifer J Sun, Jiaping Zhao, Liang-Chieh Chen, Florian Schroff, Hartwig Adam, and Ting Liu. View-invariant probabilistic embedding for human pose. In *ECCV*, pages 53–70, 2020. 1, 2
- [45] Yifan Sun, Changmao Cheng, Yuhan Zhang, Chi Zhang, Liang Zheng, Zhongdao Wang, and Yichen Wei. Circle loss: A unified perspective of pair similarity optimization. In *CVPR*, pages 6398–6407, 2020. 5, 6
- [46] Christian Szegedy, Wei Liu, Yangqing Jia, Pierre Sermanet, Scott E Reed, Dragomir Anguelov, Dumitru Erhan, Vincent Vanhoucke, and Andrew Rabinovich. Going deeper with convolutions. In *CVPR*, pages 1–9, 2015. 1
- [47] Eu Wern Teh, Terrance DeVries, and Graham W Taylor. Proxynca++: Revisiting and revitalizing proxy neighborhood component analysis. In *ECCV*, 2020. 6
- [48] Laurens Van Der Maaten. Accelerating t-sne using tree-based algorithms. *JMLR*, 15(1):3221–3245, 2014. 9
- [49] Vikas Verma, Alex Lamb, Christopher Beckham, Amir Najafi, Ioannis Mitliagkas, David Lopez-Paz, and Yoshua Bengio. Manifold mixup: Better representations by interpolating hidden states. In *ICML*, pages 6438–6447, 2019. 2
- [50] Luke Vilnis and Andrew McCallum. Word representations via gaussian embedding. In *ICLR*, 2015. 2
- [51] Catherine Wah, Steve Branson, Peter Welinder, Pietro Perona, and Serge J Belongie. The Caltech-UCSD Birds-200-2011 dataset. Technical Report CNS-TR-2011-001, California Institute of Technology, 2011. 5, 6
- [52] Hao Wang, Yitong Wang, Zheng Zhou, Xing Ji, Dihong Gong, Jingchao Zhou, Zhifeng Li, and Wei Liu. Cosface: Large margin cosine loss for deep face recognition. In *CVPR*, pages 5265–5274, 2018. 2
- [53] Jiang Wang, Yang Song, Thomas Leung, Chuck Rosenberg, Jingbin Wang, James Philbin, Bo Chen, and Ying Wu. Learning fine-grained image similarity with deep ranking. In *CVPR*, pages 1386–1393, 2014. 2
- [54] Jian Wang, Feng Zhou, Shilei Wen, Xiao Liu, and Yuanqing Lin. Deep metric learning with angular loss. In *ICCV*, pages 2593–2601, 2017. 2
- [55] Xun Wang, Xintong Han, Weilin Huang, Dengke Dong, and Matthew R Scott. Multi-similarity loss with general pair weighting for deep metric learning. In *CVPR*, pages 5022–5030, 2019. 2, 5, 6
- [56] Xinshao Wang, Yang Hua, Elyor Kodirov, Guosheng Hu, Romain Garnier, and Neil M Robertson. Ranked list loss for deep metric learning. In *CVPR*, pages 5207–5216, 2019. 6
- [57] Xun Wang, Haozhi Zhang, Weilin Huang, and Matthew R Scott. Cross-batch memory for embedding learning. In *CVPR*, pages 6388–6397, 2020. 1
- [58] Chao-Yuan Wu, R Manmatha, Alexander J Smola, and Philipp Krähenbühl. Sampling matters in deep embedding learning. In *ICCV*, pages 2859–2867, 2017. 1, 2, 4, 6, 7
- [59] Hong Xuan, Richard Souvenir, and Robert Pless. Deep randomized ensembles for metric learning. In *ECCV*, pages 723–734, 2018. 6
- [60] Lei Yang, Xiaohang Zhan, Dapeng Chen, Junjie Yan, Chen Change Loy, and Dahua Lin. Learning to cluster faces on an affinity graph. In *CVPR*, pages 2298–2306, 2019. 1
- [61] Mang Ye and Jianbing Shen. Probabilistic structural latent representation for unsupervised embedding. In *CVPR*, pages 5457–5466, 2020. 2
- [62] Baosheng Yu and Dacheng Tao. Deep metric learning with triplet margin loss. In *ICCV*, pages 6490–6499, 2019. 2
- [63] Dong Yu, Kaisheng Yao, Hang Su, Gang Li, and Frank Seide. KL-divergence regularized deep neural network adaptation for improved large vocabulary speech recognition. In *ICASSP*, pages 7893–7897, 2013. 3
- [64] Tongtong Yuan, Weihong Deng, Jian Tang, Yinan Tang, and Binghui Chen. Signal-to-noise ratio: A robust distance metric for deep metric learning. In *CVPR*, pages 4815–4824, 2019. 4
- [65] Yuhui Yuan, Kuiyuan Yang, and Chao Zhang. Hard-aware deeply cascaded embedding. In *ICCV*, pages 814–823, 2017. 2
- [66] Sangdoon Yun, Dongyoon Han, Seong Joon Oh, Sanghyuk Chun, Junsuk Choe, and Youngjoon Yoo. Cutmix: Regularization strategy to train strong classifiers with localizable features. In *ICCV*, pages 6023–6032, 2019. 2, 4
- [67] Biao Zhang and Peter Wonka. Point cloud instance segmentation using probabilistic embeddings. In *CVPR*, pages 8883–8892, 2021. 1, 2
- [68] Borui Zhang, Wenzhao Zheng, Jie Zhou, and Jiwen Lu. Attributable visual similarity learning. In *CVPR*, pages 7532–7541, 2022. 2
- [69] Hongyi Zhang, Moustapha Cisse, Yann N Dauphin, and David Lopez-Paz. mixup: Beyond empirical risk minimization. In *ICLR*, 2018. 2, 4, 5

- [70] Li Zhang, Tao Xiang, and Shaogang Gong. Learning a deep embedding model for zero-shot learning. In *CVPR*, pages 2021–2030, 2017. [1](#)
- [71] Wenliang Zhao, Yongming Rao, Ziyi Wang, Jiwen Lu, and Jie Zhou. Towards interpretable deep metric learning with structural matching. In *CVPR*, pages 9887–9896, 2021. [6](#)
- [72] Wenzhao Zheng, Zhaodong Chen, Jiwen Lu, and Jie Zhou. Hardness-aware deep metric learning. In *CVPR*, pages 72–81, 2019. [5](#)
- [73] Wenzhao Zheng, Jiwen Lu, and Zhou Jie. Structural deep metric learning for room layout estimation. In *ECCV*, 2020. [2](#)
- [74] Wenzhao Zheng, Jiwen Lu, and Jie Zhou. Deep metric learning via adaptive learnable assessment. In *CVPR*, pages 2960–2969, 2020. [2](#)
- [75] Wenzhao Zheng, Jiwen Lu, and Jie Zhou. Hardness-aware deep metric learning. *TPAMI*, 43(09):3214–3228, 2021. [2](#)
- [76] Wenzhao Zheng, Chengkun Wang, Jiwen Lu, and Jie Zhou. Deep compositional metric learning. In *CVPR*, pages 9320–9329, 2021. [1](#), [6](#)
- [77] Wenzhao Zheng, Borui Zhang, Jiwen Lu, and Jie Zhou. Deep relational metric learning. In *ICCV*, pages 12065–12074, 2021. [6](#)
- [78] Hao Zhu, Yang Yuan, Guosheng Hu, Xiang Wu, and Neil Robertson. Imbalance robust softmax for deep embedding learning. In *ACCV*, 2020. [1](#)